HHS Public Access

Author manuscript

J Am Chem Soc. Author manuscript; available in PMC 2022 June 09.

Published in final edited form as:

J Am Chem Soc. 2021 June 09; 143(22): 8314–8323. doi:10.1021/jacs.1c00290.

Visualizing the Dynamic Metalation State of New Delhi Metallo-β-lactamase-1 in Bacteria Using a Reversible Fluorescent Probe

Radhika Mehta,
Department of Chemistry, University of Texas at Austin, Austin, Texas 78712, United States

Dann D. Rivera,
Division of Chemical Biology & Medicinal Chemistry, College of Pharmacy, University of Texas, Austin, Texas 78712, United States

David J. Reilley,
Department of Chemistry and Biochemistry, University of California–Los Angeles, Los Angeles, California 90095-1569, United States

Dominique Tan,
Department of Chemistry, University of Texas at Austin, Austin, Texas 78712, United States

Pei W. Thomas,
Division of Chemical Biology & Medicinal Chemistry, College of Pharmacy, University of Texas, Austin, Texas 78712, United States

Abigail Hinojosa,
Department of Chemistry, University of Texas at Austin, Austin, Texas 78712, United States

Alesha C. Stewart,
Division of Chemical Biology & Medicinal Chemistry, College of Pharmacy, University of Texas, Austin, Texas 78712, United States

Zishuo Cheng,
Department of Chemistry and Biochemistry, Miami University, Oxford, Ohio 45056, United States

Caitlyn A. Thomas,
Department of Chemistry and Biochemistry, Miami University, Oxford, Ohio 45056, United States

Michael W. Crowder,
Department of Chemistry and Biochemistry, Miami University, Oxford, Ohio 45056, United States

Anastassia N. Alexandrova,
Department of Chemistry and Biochemistry, University of California–Los Angeles, Los Angeles, California 90095-1569, United States

Corresponding Authors Emily L. Que – Department of Chemistry, University of Texas at Austin, Austin, Texas 78712, United States; emilyque@cm.utexas.edu; **Walter Fast** – Division of Chemical Biology & Medicinal Chemistry, College of Pharmacy, University of Texas, Austin, Texas 78712, United States; walt.fast@austin.utexas.edu.

The authors declare no competing financial interest.

Supporting Information

The Supporting Information is available free of charge at https://pubs.acs.org/doi/10.1021/jacs.1c00290.

Synthetic procedures, materials and methods, and supporting figures (PDF)

Walter Fast,
Division of Chemical Biology & Medicinal Chemistry, College of Pharmacy, University of Texas, Austin, Texas 78712, United States

Emily L. Que
Department of Chemistry, University of Texas at Austin, Austin, Texas 78712, United States

Abstract

New Delhi metallo-β-lactamase (NDM) grants resistance to a broad spectrum of β-lactam antibiotics, including last-resort carbapenems, and is emerging as a global antibiotic resistance threat. Limited zinc availability adversely impacts the ability of NDM-1 to provide resistance, but a number of clinical variants have emerged that are more resistant to zinc scarcity (e.g., NDM-15). To provide a novel tool to better study metal ion sequestration in host–pathogen interactions, we describe the development of a fluorescent probe that reports on the dynamic metalation state of NDM within *Escherichia coli*. The thiol-containing probe selectively coordinates the dizinc metal cluster of NDM and results in a 17-fold increase in fluorescence intensity. Reversible binding enables competition and time-dependent studies that reveal fluorescence changes used to detect enzyme localization, substrate and inhibitor engagement, and changes to metalation state through the imaging of live *E. coli* using confocal microscopy. NDM-1 is shown to be susceptible to demetalation by intracellular and extracellular metal chelators in a live-cell model of zinc dyshomeostasis, whereas the NDM-15 metalation state is shown to be more resistant to zinc flux. The development of this reversible turn-on fluorescent probe for the metalation state of NDM provides a new tool for monitoring the impact of metal ion sequestration by host defense mechanisms and for detecting inhibitor–target engagement during the development of therapeutics to counter this resistance determinant.

Graphical Abstract

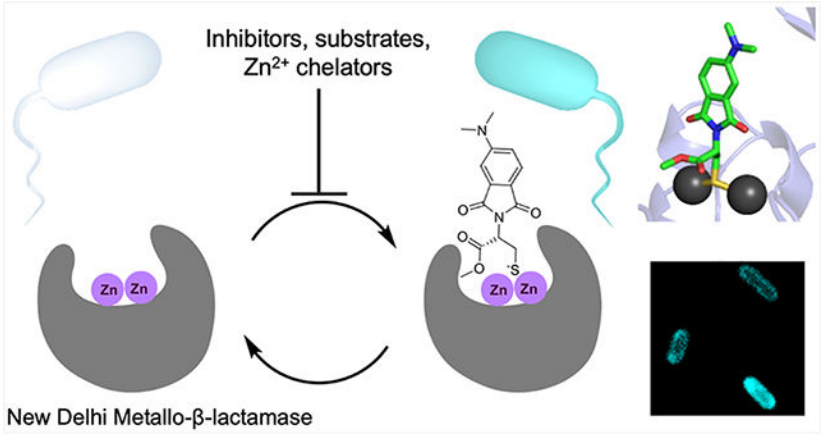

INTRODUCTION

New Delhi metallo-β-lactamases (NDM) are an emerging global antibiotic resistance threat with the ability to hydrolyze and thereby inactivate almost all clinically used β-lactam drugs, including last-resort carbapenems.[1,2] First identified in 2008,[3] NDM-1 is a dizinc

metalloprotein with broad substrate promiscuity encompassing a wide range of penicillins, cephalosporins, and carbepenems.[4-6] The metal cluster is comprised of two zinc ions, with the first (Zn1) coordinated to three histidines and the second (Zn2) coordinated to an aspartate, a cysteine, and a histidine, and both zinc ions bridged by a nucleophilic hydroxide ion.[7] The binding constants for each zinc site are quite disparate ($K_{d,Zn1} \approx 1$ nM; $K_{d,Zn2} \approx 1$ μM) when measured using a soluble mutant of NDM-1 that lacks an *N*-terminal lipidation sequence.[8] Characterization of emerging clinical variants of NDM (NDM-1 through NDM-17) revealed that many of these mutations impart enhanced affinity for Zn2 (e.g., NDM-15 $K_{d,Zn2} = 120$ nM) and likely arose due to the dual selective pressures of antibiotic treatment and zinc scarcity.[8-10] Lipidation of full-length NDM-1 tethers the enzyme to the inner leaflet of the outer membrane and increases zinc affinity, but this form of NDM-1 still remains notably more susceptible to ampicillin in the presence of metal chelators than NDM variants with increased Zn2 affinity.[8,11] The weak affinity of NDM-1 for Zn2 appears to be a vulnerability likely exploited both by infected hosts through nutritional immunity and by design of β-lactam:chelator co-drug strategies.[12,13]

At the host–pathogen interface, nutritional immunity can use metal dyshomeostasis to adversely impact bacterial survival through sequestration of zinc, manganese, iron, and other metal ions.[14-17] The metalation of other metallo-β-lactamases is dependent on extracellular metal ion identity and concentration.[18] Resistance imparted by NDM[11,19] and other multi-drug-resistant bacterial systems[20,21] is adversely impacted by chelation of extracellular zinc by the host-derived protein calprotectin[11,20,22] or exogenously added small-molecule chelators.[23] However, detecting the metalation state of NDM and its clinical variants during these challenges is not straightforward and usually relies on the use of purified components or on measurements of enzyme activity or bacterial growth. To better study the interplay of nutritional immunity and NDM in antibiotic resistance, we sought to develop a new tool to directly monitor the metalation state of NDM *in situ*.

Previously, we studied models of zinc dyshomeostasis in HeLa cells by designing small-molecule fluorescent probes that report on the metalation status of intracellular carbonic anhydrase.[24] Some existing NDM-1 targeted fluorophores consist of fluorogenic substrates[25,26] or covalent modifiers[27,28] and represent irreversible “switch on” probes. However, these probes do not necessarily report on metalation and lack the ability to monitor dynamic reversible changes. Herein, we developed a reversible fluorescent detector for NDM metalation by coupling an environmentally sensitive fluorescent reporter to a thiol-containing moiety similar to those contained in previously reported NDM inhibitors.[29,30,31] Thiol-based inhibitors are a well-established inhibitor type for metallo-β-lactamases in which the thiol displaces the nucleophilic hydroxide ion and forms a new bridge between Zn1 and Zn2.[6] The base of the neighboring substrate-binding β-hairpin loop consists of hydrophobic residues, which contrast with the aqueous solvent and provide a much different environment for the bound fluorophore.[6] Using this approach, we report the development and characterization of a reversible fluorescent probe selective for the holo dizinc form (metalloform) of NDM-1 and demonstrate its use in confocal microscopy to visualize the dynamic metalation states of clinical NDM variants in live bacteria when challenged by zinc sequestration agents as a model of nutritional immunity.

RESULTS AND DISCUSSION

Synthesis and Photophysical Properties of the Synthesized Probes.

To make a fluorescent probe specific for dizinc NDM-1, we linked the environment-sensitive fluorophore 4-*N,N*-dimethylaminopthalimide (**4-DMAP**)[32] with thiol derivatives predicted to bind NDM-1 with micromolar affinity via direct interactions with both Zn^{2+} ions in the enzyme active site (Figure 1). These small-molecule fluorescent probes for NDM-1 (Figure 1B) were synthesized in multiple steps from *N,N*-dimethylaminophthalic anhydride (**DMAP**).[24,33] Here, **DMAP** was coupled with cysteamine to generate probe **1**. Probe **2**, using glycine as a precursor, was generated to compare interactions with a nonthiol-based metal binding group. To facilitate potential active-site hydrogen-bonding interactions, we also synthesized cysteine-containing probes incorporating both the thiol and carboxylate moieties. Probes **3D** and **3L** were synthesized by combining D- or L-cysteine precursors with **DMAP** in refluxing acetic acid. Lastly, the methyl esters of **3D/3L** were synthesized by reacting **3D/3L** with thionyl chloride in methanol to afford **4D/4L** in 68% and 50% yields, respectively. The probes were characterized for purity using ^{1}H NMR, ^{13}C NMR, and HRMS. All the probes displayed similar spectroscopic characteristics, with λ_{ex} = 417–420 nm and λ_{em} = 575–580 nm in HEPES buffer. The quantum yields and extinction coefficients of probes **1–4L** in methanol are provided in Table S1.

Fluorescence Response and Inhibition of NDM-1 with Probes 3D and 4D.

Fluorescence spectroscopy studies of probes **1–4L** following incubation with NDM-1 (Figure 1C) were performed in aqueous buffer supplemented with 10 μM $ZnSO_4$. Probes **1** and **2** displayed 6- and 1.2-fold fluorescence turn-on, respectively, with NDM-1, indicating that the thiol group in probe **1** is important for interaction with NDM-1, as has been reported previously.[29,34] The cysteine derivatives **3D** and **3L** displayed up to 15- and 11-fold turn-on, respectively, upon addition of NDM-1. These increases in fluorescence are accompanied by 33 nm (**3D**) and 31 nm (**3L**) hypsochromic shifts in λ_{em} from 575 nm (Figure S1A,B). The cysteine methyl ester derivatives **4D** and **4L** showed 12- and 6-fold turn-on in fluorescence with NDM-1, respectively, along with 50 and 58 nm hypsochromic shifts in λ_{em} from 575 nm (Figure 1D, Figure S1C). Among the four probes, **4L** showed the highest shift in λ_{em}, followed by **4D**, indicating that the ester-based probes experience more hydrophobic interactions with nonpolar regions of the NDM-1 active site compared to **3D/3L**. The larger turn-on for the D-forms (**3D, 4D**) indicates differences in binding and fluorescence response, which are attributed to multiple factors including polarity, electrostatics, and sterics (Figure S2). The preference of NDM-1 for one isomer over another is precedented. The well-studied NDM-1 inhibitor captopril shows differences in IC_{50} values between its isomers, with the D-form having a stronger interaction with NDM-1 (IC_{50} D-captopril: 7.9 μM versus L-captopril: 202 μM).[7] We hypothesize that, similar to D-captopril, the thiol group in **3D/4D** likely serves as a bridging ligand between Zn1 and Zn2 and the carboxylate/ester group facilitates binding through secondary interactions with the active-site binding pocket, further stabilizing the probe:NDM-1 interaction. We measured an IC_{50} of 6.3 ± 0.2 μM for probe **4D** and NDM-1 (Figure S3). The IC_{50} value for **4D** is similar in magnitude to that of D-captopril and previously reported thiol-containing NDM-1 inhibitors.[31] Assuming competitive inhibition and fixing the substrate (chromacef) concentration (20 μM; K_m = 0.66 ± 0.20 μM[35]), a K_i of

200 ± 30 nM can be calculated for the **4D**:dizinc NDM-1 interaction.[36] Despite structural similarity to **4D**, the probe **3D** did not fully abrogate activity (Figure S3), indicating likely differences in the binding interactions made between NDM-1 and **3D** and **4D**. Because of its superior inhibitory characteristics, most of our subsequent studies focused on **4D**.

To better understand the differences between NDM-1 binding interactions with **3D, 4D**, and L-captopril, we conducted computational simulations using a QM/DMD method[37-39] (Figure 2, Figure S4). These simulations assessed different potential binding modes between the probes and NDM-1 (Figure S16). The calculated binding mode for both **3D** and **4D** places the thiol group as a bridging Zn1 and Zn2 ligand, similar to that reported with L-captopril from crystal structures.[6] The lowest energy exemplary structure for bound **4D** demonstrates this conformation and is shown in Figure 2. This pose reflects hydrophobic interactions made between the fluorophore end and a methionine residue (M67) in the substrate-binding β-hairpin loop of NDM-1 which may contribute to the fluorescence response of this probe (Figure 2A). The calculated probe binding penalty is larger for **3D** (10.5 kcal/mol) than **4D** (4.2 kcal/mol), though both are smaller than the value calculated for L-captopril (19.5 kcal/mol) based on its crystal structure (PDB ID: 4EXS).[6] This result predicts that **4D** is less readily unbound and solvated than **3D** or L-captopril and therefore binds more tightly to the NDM-1 active site, consistent with the lower measured IC_{50} value. This difference in affinity likely arises from a stronger binding of the probe to the metals due to a better geometry and more favorable active-site interactions. Calculated metal angle variances, which are a measure of unfavorable deviations of the Zn coordination from the ideal tetrahedral (Table 1, Figure S17), show that the lowest energy structure for **3D** reports a somewhat larger deviation from the ideal zinc tetrahedral geometry at 7.96° versus 7.52° for **4D**, contributing to poorer binding of **3D**. Assessment of the average metal angle variance across the full ensemble of states shows a larger difference of 10.77 ± 1.73° versus 8.32 ± 1.10°, with **3D** metal geometry being typically much worse than that of **4D**. Figure 2B,C shows hydrogen-bonding interactions between asparagine (N220) and lysine (K211) residues and the carbonyl groups within the fluorophore and metal-binding group of the probe, respectively (Figures S18 and S20). While the lengths of these hydrogen-bonding interactions are similar between the lowest energy structures for **3D** and **4D**, analysis of the full ensemble of states shows that a direct probe:Lys 178 hydrogen bond occurs about 38% more often in **4D** than in **3D** (Figure S19). A more thorough discussion of these analyses and graphs (Figures S16-S24) of the full ensembles of states can be found in the Supporting Information.

To further support our theory of thiol–metal coordination at the active site, we synthesized the thioether derivative of **4D, 4D-SMe**. **4D-SMe** displayed no fluorescence response with NDM-1, indicating that thiol alkylation prevents interaction with the protein (Figure S1D). We also performed spectroscopic studies with cobalt-substituted NDM-1 (CoCo-NDM-1) to monitor changes in its UV–vis spectrum upon probe binding.[40-42] Due to the inherent absorption of **4D** at 342 nm, which obscures observation of thiolate-Co LMCT transitions, we monitored CoCo-NDM-1 absorbance peaks between 500 and 600 nm, which are attributed to the ligand field (d-d) transitions of high-spin Co(II). Addition of 1 equiv of **4D** to CoCo-NDM-1 (Figure S5) resulted in changes in the shape of the ligand field transitions, similar to what has been previously observed upon addition of captopril to CoCo-

NDM-1,[35,43,44] and consistent with a μ-sulfido-bridged binding mode between **4D** and NDM-1. Further, the absence of ligand field transitions in the spectrum of apo-NDM-1 with 1 equiv of **4D** confirmed that the observed changes for CoCo-NDM-1 with **4D** were due to interaction of **4D** with the metal ions, and not due to **4D** alone. These results strongly support direct thiolate coordination of **4D** to the metal sites of NDM-1.

Reversibility and Selectivity Profile of Probe 4D.

We next studied the effect of $ZnSO_4$ and chelators on the fluorescence response between **4D** and NDM-1. Addition of up to 50 μM $ZnSO_4$ to **4D** and purified NDM-1 *in vitro* led to an increase in fluorescence turn-on to give an overall ~17-fold response (Figure 3B). This indicates that more exogenous zinc is required under these conditions to fully metalate dizinc NDM-1, since at lower zinc supplementation (10 μM) the fluorescence response was lower. This 17-fold response represents the maximum turn-on in which **4D** is fully bound to the NDM-1 metalloform, as addition of more protein did not increase this response. In contrast, incubation of **4D** with monozinc NDM-1, formed via pretreatment with 4-(2-pyridylazo)resorcinol (PAR),[5] led to a 70% reduction in observed fluorescence intensity relative to the same sample without PAR treatment or zinc supplementation, indicating that occupancy of the weaker binding Zn2 site is essential for the large fluorescence increase of 4D upon binding (Figures S6A). As a control, we also measured the fluorescence of probe **4D** in the presence of $ZnSO_4$ only (up to 50 μM, Figure S6B) and observed no change in fluorescence. Based on these results, we conclude that probe **4D** can be employed to specifically detect the holo dizinc-NDM-1 metalloform *in vitro*.

Next, to test the ability of **4D** to detect dynamic changes in the NDM-1 metalation state or active-site occupancy, we performed several challenge studies. Treatments of the fluorescent **4D**:NDM-1 complex with the competitive inhibitor DL-captopril, the zinc chelator *N,N,N′,N′*-tetrakis(2-pyridinyl-methyl)-1,2-ethanediamine (TPEN), and the inhibitor dipicolinic acid (DPA) (which has an inhibition mechanism that includes both NDM binding and zinc sequestration[35]) all resulted in a decrease in observed fluorescence (Figure 3A,B). With DL-captopril (200 μM), we observed the fluorescence turn-on decrease from the 17-fold maximum to ~13-fold (Figure 3B). This partial decrease is consistent with probe **4D** having a stronger affinity for NDM-1 than the DL-captopril mixture (IC_{50} D-captopril: 7.9 μM versus L-captopril: 202 μM)[7] and thus only partially displaces **4D** from the active site. Treatment with DPA (150 μM, $IC_{50,NDM-1}$ = 154 μM at 50 μM $ZnSO_4$ Figure S7) resulted in a similar decrease in fluorescence turn-on to 13-fold (Figure 3B), consistent with the weaker affinity of DPA for NDM-1. Lastly, with the addition of TPEN (50 μM) to the **4D**:NDM-1 complex (now in 10 μM $ZnSO_4$ to not overwhelm the chelator), we observed that the fluorescence turn-on decreased from 12-fold to 9.2-fold (Figure 3B). TPEN (Zn^{2+}, $K_d = 10^{-16}$ M;45 $IC_{50,NDM-1}$ = 0.088 μM[46]) can cause demetalation of NDM-1 and result in loss of probe binding. The lack of complete fluorescence loss may be due to the inability of TPEN to access the active site when the probe is bound under these conditions. To test this hypothesis, we pre-incubated 30 μM NDM-1 with TPEN, followed by addition of 10 μM **4D** that resulted in a much larger reduction in intensity, down to ~4-fold (Figure S6C). Additionally, to determine if we can completely quench the fluorescence, we performed the pre-incubation studies at 10 μM NDM-1 and 10 μM **4D**, thus eliminating excess NDM-1.

Figure S6D shows complete reduction of fluorescence that is then recovered upon addition of excess $ZnSO_4$. Reduction in fluorescence following the chelation of zinc suggests that the probe (**4D**) can report on the availability of the holo dizinc NDM-1 metal site and can be used either as a probe to detect competitive ligand binding or to detect changes in metalation state.

To test probe selectivity, **4D** was incubated with other proteins, including bovine and human carbonic anhydrase II (bCAII, hCAII), myoglobin, Cu,Zn-superoxide dismutase (Cu,Zn-SOD), dizinc enzymes alkaline phosphatase (AKP) and phosphotriesterase (PTE), and bovine serum albumin (BSA). Of significance here is the ~22-fold fluorescence response with PTE, another dizinc enzyme and a potential off-target. However, it is important to note that PTE is found in soil bacteria and not in *E. coli*, where we perform our cell experiments.[47] However, we note that no fluorescence turn-on was observed with the other dizinc enzyme, AKP. A small fluorescence turn-on (4–5-fold) with hCAII and BSA was observed (Figure 3C). The fluorescence of **4D** was quenched when **4D** was combined with myoglobin. BSA is known to interact strongly with probes containing carboxylic groups.[48,49] Consistent with this trend, the carboxylate-containing probe **3D** gave up to an 85-fold increase in fluorescence when bound to BSA (data not shown), but the neutral ester-containing probe **4D** showed only a minimal 3-fold increase (Figure 3C). This panel of representative proteins indicates that, while **4D** may not be completely selective for NDM-1, it is crucial to test its specificity in the biological context in which the probe is applied, as is true with other biologically applied fluorescent sensors.

Next, we tested **4D** with purified forms of two clinically significant metallo-β-lactamases that share amino acid sequence identity to NDM-1: VIM-2 (35%) and IMP-1 (28%). VIM-2 and IMP-1 displayed 6- and 3.8-fold fluorescence turn-on, respectively, with probe **4D**. While many metallo-β-lactamases have the conserved dizinc metal cluster and similar hydrophobic patches neighboring the active site, differences in the surrounding sequence likely result in environments with less ability to enhance **4D** fluorescence than NDM-1. Addition of 50 μM $ZnSO_4$ to these incubations led to a minor increase in fluorescence turn-on to 8-fold for VIM-2 and a decrease to 3.5-fold turn-on for IMP-1. The small increase (or decrease) in fluorescence turn-on observed with $ZnSO_4$ is consistent with the tighter Zn2 affinity of these enzymes.[41,50]

Many clinical variants of NDM-1 have evolved in response to zinc deprivation.[8-10] We compared four purified NDM variants with differing Zn2 affinity for characterization with **4D**: NDM-1 (reference sequence, $K_{d,Zn2}$ = 1 μM), NDM-4 (M154L, $K_{d,Zn2}$ = 230 nM), NDM-6 (A233V, $K_{d,Zn2}$ = 310 nM), and NDM-15 (M154L, A233V, $K_{d,Zn2}$ = 120 nM).[8] Each of these mutations is distant from the dizinc cluster and not likely to directly perturb the hydrophobic character of the active site. NDM-4 and NDM-6 showed 12- and 13-fold fluorescence turn-on, and, like NDM-1, their turn-on increased with addition of more exogenous zinc. The results of NDM-15 contrast with those of the other variants and yielded the highest fluorescence turn-on of 17-fold (Figure 3D), which only increased to 17.8-fold upon addition of 50 μM $ZnSO_4$. These results are consistent with the selectivity of probe **4D** specifically for the holo dizinc metalloform of NDM, which is more favored in the NDM-15 variant due to increased Zn2 affinity. Overall, these results indicate that fluorescence turn-on

of **4D** is dependent on the NDM active site being fully metalated, at which point we observe ~17–18-fold fluorescence turn-on, indicating the usefulness of **4D** to monitor the dynamic metalation status of NDM.

Application of 4D in Cells and Cell Lysates.

Building on these *in vitro* studies, we characterized **4D**:NDM-1 interactions in live bacteria via confocal microscopy and in cell lysates via in-gel fluorescence staining using native SDS-PAGE.[24] As seen in Figure 4A, BL21 (DE3) *E. coli* cells expressing Δ35 NDM-1 (see description of this construct below) exhibit bright fluorescence staining when incubated with **4D**. Conversely, no fluorescence is observed in the absence of IPTG when NDM-1 is not expressed (Figure 4A), which is an important observation supporting lack of off-target response in this cellular context. These results are consistent with the association of **4D** turn-on fluorescence with the expression of periplasmically directed NDM and consistent with the bioavailability of **4D** to proteins within the bacteria. We observed a single fluorescent band in the native SDS-PAGE of cell lysates from NDM-1-expressing cells containing **4D** (Figure 4B). These results indicate that one major protein band is visualized using **4D**, and the mobility of this band corresponds with purified NDM-1, demonstrating selectivity of the probe for NDM-1 in this biological context. We note that, as a control, we incubated mammalian cells (MCF-7) with **4D** and observed staining throughout the intracellular milieu (Figure S8), indicating that this probe is not selective for NDM-1 in this context. This highlights the importance of performing appropriate control experiments when applying chemical probes in biological contexts.

Three types of NDM-1 constructs were cloned into a pET-27b host vector after an IPTG-inducible T7 promoter and assessed for their interactions with **4D** in *E. coli*. Full-length NDM-1 (FL) includes the native *N*-terminal leader sequence containing the periplasmic signal peptide and a lipidation signal as well as a C-terminal His_6-affinity tag.[5] This lipidation localizes NDM-1 to the inner leaflet of the outer membrane, placing the NDM catalytic domain within the periplasmic space.[11] C26A NDM-1 (C26A) is encoded by the same construct as FL, but the Cys targeted for lipidation is mutated to an Ala to prevent modification. This mutation leads to accumulation of water-soluble C26A NDM-1 in the periplasmic space.[11] Δ35 NDM-1 contains a 35-amino-acid *N*-terminal truncation used to generate a water-soluble form of NDM used in our *in vitro* studies and is preceded by a pelB leader sequence to direct export to the periplasm, followed by a Strep-tag II affinity tag that precedes the NDM sequence.[5]

After treatment of *E. coli* expressing FL NDM-1 with **4D**, fluorescence around the cell periphery was observed, consistent with the expected periplasmic localization of the enzyme and similar to immunostained images of FL NDM-1 previously reported.[11] After long incubation times (>2 h), some cells start displaying punctate fluorescence patterns at the poles of the cells. Similar patterns were reported previously with Cys-reactive covalent fluorescent probes of NDM-1 and were attributed to accumulation of aggregated proteins,[27,51] although the experiments described below are more consistent with those regions also containing active, folded, dizinc NDM-1. *E. coli* cells expressing the C26A NDM-1 construct showed a similar pattern after treatment with **4D**. However, the punctate features at

the poles are more prominent, again similar to previously reported immunostained images of C26A-expressing cells. [11] **4D** treatment of the strain expressing Δ35 NDM-1 showed even more fluorescence at the poles (Figure 4C, Figure S9). We also employed **4D** for visualizing NDM-1 expressed constitutively in E. *coli* DH5a cells at levels similar to those of clinical variants (using the pHSG298 vector[9]). We observed peripheral fluorescence in ~60% of the cells, consistent with periplasmic localization and demonstrating the utility of our probe in systems where NDM-1 is not overexpressed (Figure S10).

Visualizing the Dynamic Metalation State of NDM-1 in Bacteria.

We focused on Δ35 NDM-1 for the remaining experiments because the activities of soluble NDM variants are more sensitive to zinc chelators than those of lipidated NDM, and we sought to monitor the construct with the widest range of accessible metalation states. To rule out the possibility that the observed fluorescence turn-on of **4D** in Δ35 expressing cells arises merely from partitioning into hydrophobic regions of unfolded, aggregated proteins at the poles of the bacteria, we tested whether **4D** could be displaced by specific NDM-1 substrates and inhibitors. As shown in the schematic in Figure 5A, we expected that high concentrations of a β-lactam substrate would temporarily displace the probe and lead to a decrease in fluorescence. As the substrate concentration is decreased by enzymatic hydrolysis to product, we expected that **4D** would be able to outcompete and rebind to the active site of NDM-1, thereby leading to recovery of the fluorescence signal. As predicted, addition of excess cephalexin (1 mM; K_m = 5.6 μM; $k_{cat}/K_m = 8.4 \times 10^6$ M^{-1} s^{-1})[5] caused a brief reduction in fluorescence of Δ35 NDM-1 expressing BL21 (DE3) *E. coli*, followed by an increasing fluorescence to a value near that preceding addition of the substrate (Figure 5B,C). Figure 5C shows representative images of cells in this experiment, showing an obvious increase in intensity at the poles over time where most of the fluorescence is localized. We also monitored total cellular NDM-1 expression over the same time points; NDM-1 levels did not change over this time period (Figure S11). The ability to monitor reversible changes in NDM active-site accessibility highlights a design feature of using a reversible probe rather than some previously employed covalent tagging reagents. These results also support our interpretation that the punctate accumulation of NDM at the poles of the cell contains active, folded, dizinc protein rather than only aggregated misfolded proteins. Although the probe was designed to probe metalation state, we also recognize its ability to validate target engagement by NDM ligands in the cell.

To further test this application, we used **4D** as a reporter to monitor target engagement by the inhibitor DL-captopril. D-Captopril has previously been shown to lower the minimum inhibitor concentration (MIC) of meropenem in NDM-1 expressing cells, so this compound can likely gain access to the periplasmic space.[52] We treated Δ35 NDM-1 expressing BL21 (DE3) *E. coli* with **4D** and then with increasing concentrations of DL-captopril (Figure 5D, Figure S12). The resulting fluorescence intensity decreased in a dose-dependent manner, indicating that this NDM inhibitor can effectively compete with **4D** for binding.

To apply **4D** as a probe of NDM metalation status in *E. coli*, we studied the differential effects of three types of metal chelators on observed fluorescence: DPA, TPEN, and CaEDTA. Treatment by DPA requires approximately 200 μM (Figure 5E, Figure S13) to

achieve a 50% decrease in fluorescence, with the decrease presumably representing a combination of displacing **4D** from the active site and zinc sequestration. This required concentration is much larger than the IC_{50} of DPA for purified NDM-1 (0.5 μM),[35] since DPA is known to weakly chelate a wide range of divalent metal ions[53] that are present in cells and imaging media (10^{-2}–10^{-7} M). We then monitored the effect of the membrane-permeable, strong zinc chelator ($K_{d,\,Zn(II)} = 10^{-16}$ M)[45] TPEN (10 and 50 μM) over 15–20 min. We observed a concentration-dependent change in fluorescence intensity that decreased by ~66% with 50 μM TPEN (Figure 5F, Figure S14). TPEN does not resemble NDM-1 inhibitors and likely acts here solely as a zinc sequestration agent that decreases fluorescence by preventing formation of the **4D**:NDM complex. Finally, we mimicked external zinc sequestration by using an extracellular zinc chelator,[54] calcium EDTA (CaEDTA). Addition of 10 μM CaEDTA ($K_{d,Zn(II)} = 10^{-9}$ M)[54] showed no significant decrease in fluorescence (Figure 5G, Figure S15). However, higher CaEDTA concentrations (50 μM) decreased the fluorescence intensity by ~33%. A number of reports have indicated increased susceptibility of NDM-1 expressing *E. coli* to antibiotics upon treatment with EDTA (for one example, see ref 8). However, EDTA can increase the outer membrane permeability,[55] so it is not entirely clear whether the increases in susceptibility are due to zinc sequestration or to increasing periplasmic access. Here, we use the probe **4D** to demonstrate that NDM-1 is demetalated by treatment with exogenous zinc chelators, supporting zinc sequestration as the likely mechanism for increased susceptibility.

Comparing Metalation Status between Clinical Variants of NDM.

Since the discovery of NDM in 2008, more than 30 allelic variants of NDM have emerged.[56] While many of these variants do not show appreciably improved kinetic constants for β-lactam hydrolysis or resistance to inhibitors, a large proportion of the variants have lower $K_{d,Zn2}$ values and an associated increase in thermostability.[8-10,57] NDM variants with increased Zn2 affinity can outcompete other variants when grown in environments with low zinc availability.[8-10] NDM-15 has one of the most improved $K_{d,Zn2}$ values characterized to date.[8] We compared the ability of probe **4D** to visualize Δ35 NDM-1 and the variant Δ35 NDM-15 when expressed and exported to the periplasm of *E. coli*. The localization of Δ35 NDM-15 was similar to that of Δ35 NDM-1 but showed more fluorescence around the cell periphery (Figure 6A), consistent with less trapping of this variant within unfolded proteins at the poles and the increased thermostability of this variant.[8,10,57] Despite these similarities, challenges of these strains by zinc chelators showed marked differences. Treatment with TPEN and DPA resulted in markedly smaller changes in fluorescence intensity for NDM-15 than NDM-1 (Figure 6B, Figures S13 and S14). TPEN, a stronger zinc chelator, only decreased the fluorescence by ~30% at 50 μM concentration. DPA treatment had no effect on fluorescence, even at 200 μM. This clearly indicates that NDM-15 is more resistant to the rapid demetalation observed with NDM-1, even to membrane-permeable chelators.

CONCLUSIONS

We report the development of a novel probe, **4D**, to monitor the dynamic metalation state of NDM within *E. coli*. Coupling of an environment-sensitive fluorophore to a thiol-based NDM inhibitor scaffold resulted in an active-site-directed ligand that achieves a 17-fold

fluorescence turn-on upon binding NDM-1. Binding of the probe is reversible—it can be displaced either by competition with non-fluorescent active-site ligands or by demetalation of NDM, with the resulting loss in fluorescence enabling monitoring of dynamic alterations to the active-site metal content. The probe is shown to be specific for NDM in *E. coli* by native gel electrophoresis with cell lysates and absence of any fluorescence in cells lacking NDM-1 expression. Notably, the probe can be used with confocal microscopy to image dizinc NDM expressed in the *E. coli* periplasm and can report on dynamic changes in ligand binding during substrate and inhibitor engagement with NDM as well as during demetalation by both cell-permeable and cell-impermeable zinc chelators. In comparison with NDM-1, the clinical variant NDM-15 is shown to be more resistant to demetalation by zinc chelators than NDM-1 in cells, consistent with decreases in antibiotic susceptibility when resistant strains are grown under zinc-deficient conditions. These experiments establish **4D** as a useful probe for dynamically monitoring NDM metalation state and active-site occupancy in bacteria for the study of metal ion sequestration in host–pathogen interactions, evolution of more resistant enzyme variants, and the development of novel NDM-directed therapeutics to counter the rising threat of carbapenem-resistant Enterobacteriaceae. This novel imaging tool can be particularly useful for screening new inhibitors for NDM and ascertaining the efficacy of target engagement *in vivo*. Future work will include the development of higher-specificity probes with optimized active-site interactions that can be applied in more complex biological samples.

Supplementary Material

Refer to Web version on PubMed Central for supplementary material.

ACKNOWLEDGMENTS

Confocal imaging was performed at the ICMB Microscopy and Imaging Facility at UT Austin. We would like to thank Anna Webb for confocal training and helpful discussions for bacteria imaging. The substrate chromacef was a generous gift from Larry Sutton (Benedictine College, Atchison, KS). Phosphotriesterase was a generous gift from Prof. Frank Raushel and Dao Xiang (Texas A&M, College Station, TX).

Funding

This work was supported in part by the National Institutes of Health (Grant R35 GM133612 E.L.Q; GM111926 to W.F.; GM134047 to A.N.A.; GM134454 to M.W.C.), the National Science Foundation (grant CHE-1903808 to A.N.A.) and by the Robert A. Welch Foundation (Grant F-1883 to E.L.Q; F-1572 to W.F.). Some NMR spectra were acquired on Bruker AVIII HD 500 instrument acquired through a National Institutes of Health equipment grant (J. Sessler, 1 S10 OD021508-01).

ABBREVIATIONS

NDM	New Delhi metallo-β-lactamase
TCEP	tris(2-carboxyethyl)phosphine
TPEN	*N,N,N′,N′*-tetrakis(2-pyridinylmethyl)-1,2-ethanediamine
DPA	dipicolinic acid
PAR	4-(2-pyridylazo)resorcinol

CA	carbonic anhydrase
MIC	minimum inhibitor concentration
BSA	bovine serum albumin

REFERENCES

(1). Linciano P; Centron L; Gianquinto E; Spyrakis F; Tondi D Ten Years with New Delhi Metallo-β-Lactamase-1 (NDM-1): From Structural Insights to Inhibitor Design. ACS Infect. Dis 2019, 5, 9. [PubMed: 30421910]

(2). Dortet L; Poirel L; Nordmann P Worldwide dissemination of the NDM-type carbapenemases in Gram-negative bacteria. BioMed Res. Int 2014, 2014, 249856. [PubMed: 24790993]

(3). Yong D; et al. Characterization of a new metallo-beta-lactamase gene, bla(NDM-1), and a novel erythromycin esterase gene carried on a unique genetic structure in *Klebsiella pneumoniae* sequence type 14 from India. Antimicrob. Agents Chemother 2009, 53, 5046. [PubMed: 19770275]

(4). Sun Z; Hu L; Sankaran B; Prasad BVV; Palzkill T Differential active site requirements for NDM-1 β-lactamase hydrolysis of carbapenem versus penicillin and cephalosporin antibiotics. Nat. Commun 2018, 9, 4524. [PubMed: 30375382]

(5). Thomas PW; et al. Characterization of Purified New Delhi Metallo-β-lactamase-1. Biochemistry 2011, 50, 10102. [PubMed: 22029287]

(6). King DT; Worrall LJ; Gruninger R; Strynadka NC New Delhi metallo-β-lactamase: structural insights into β-lactam recognition and inhibition. J. Am. Chem. Soc 2012, 134, 11362. [PubMed: 22713171]

(7). Guo Y; et al. A structural view of the antibiotic degradation enzyme NDM-1 from a superbug. Protein Cell 2011, 2, 384. [PubMed: 21637961]

(8). Cheng Z; et al. Evolution of New Delhi metallo-β-lactamase (NDM) in the clinic: Effects of NDM mutations on stability, zinc affinity, and mono-zinc activity. J. Biol. Chem 2018, 293, 12606. [PubMed: 29909397]

(9). Stewart AC; et al. Clinical Variants of New Delhi Metallo-β-Lactamase Are Evolving To Overcome Zinc Scarcity. ACS Infect. Dis 2017, 3, 927. [PubMed: 28965402]

(10). Bahr G; Vitor-Horen L; Bethel CR; Bonomo RA; González LJ; Vila AJ Clinical Evolution of New Delhi Metallo-β-Lactamase (NDM) Optimizes Resistance under Zn(II) Deprivation. Antimicrob. Agents Chemother 2017, 62, e01849–17. [PubMed: 29038264]

(11). González LJ; Bahr G; Nakashige TG; Nolan EM; Bonomo RA; Vila AJ Membrane anchoring stabilizes and favors secretion of New Delhi metallo-β-lactamase. Nat. Chem. Biol 2016, 12, 516. [PubMed: 27182662]

(12). Falconer SB; et al. Zinc Chelation by a Small-Molecule Adjuvant Potentiates Meropenem Activity in Vivo against NDM-1-Producing Klebsiella pneumoniae. ACS Infect. Dis 2015, 1, 533. [PubMed: 27623408]

(13). Worthington RJ; Melander C Combination approaches to combat multidrug-resistant bacteria. Trends Biotechnol. 2013, 31, 177. [PubMed: 23333434]

(14). Becker KW; Skaar EP Metal limitation and toxicity at the interface between host and pathogen. FEMS Microbiol. Rev 2014, 38, 1235. [PubMed: 25211180]

(15). Hood MI; Skaar EP Nutritional immunity: transition metals at the pathogen-host interface. Nat. Rev. Microbiol 2012, 10, 525. [PubMed: 22796883]

(16). Wątły J; Potocki S; Rowińska-Żyrek M Zinc Homeostasis at the Bacteria/Host Interface-From Coordination Chemistry to Nutritional Immunity. Chem. - Eur. J 2016, 22, 15992. [PubMed: 27555527]

(17). Begg SL The role of metal ions in the virulence and viability of bacterial pathogens. Biochem. Soc. Trans 2019, 47, 77. [PubMed: 30626704]

(18). Hu Z; Gunasekera TS; Spadafora L; Bennett B; Crowder MW Metal content of metallo-beta-lactamase L1 is determined by the bioavailability of metal ions. Biochemistry 2008, 47, 7947. [PubMed: 18597493]

(19). Meini MR; González LJ; Vila AJ Antibiotic resistance in Zn(II)-deficient environments: metallo-β-lactamase activation in the periplasm. Future Microbiol. 2013, 8, 947. [PubMed: 23902139]

(20). Wang J; et al. Multi-metal Restriction by Calprotectin Impacts De Novo Flavin Biosynthesis in Acinetobacter baumannii. Cell Chem. Biol 2019, 26, 745. [PubMed: 30905682]

(21). Chan AN; Shiver AL; Wever WJ; Razvi SZ; Traxler MF; Li B Role for dithiolopyrrolones in disrupting bacterial metal homeostasis. Proc. Natl. Acad. Sci. U. S. A 2017, 114, 2717. [PubMed: 28209778]

(22). Zygiel EM; Nolan EM Transition Metal Sequestration by the Host-Defense Protein Calprotectin. Annu. Rev. Biochem 2018, 87, 621. [PubMed: 29925260]

(23). Siemann S; Brewer D; Clarke AJ; Dmitrienko GI; Lajoie G; Viswanatha T IMP-1 metallo-beta-lactamase: effect of chelators and assessment of metal requirement by electrospray mass spectrometry. Biochim. Biophys. Acta, Gen. Subj 2002, 1571, 190.

(24). Mehta R; et al. A new probe for detecting zinc-bound carbonic anhydrase in cell lysates and cells. Chem. Commun 2018, 54, 5442.

(25). Mao W; Wang Y; Qian X; Xia L; Xie H A Carbapenem-Based Off–On Fluorescent Probe for Specific Detection of Metallo-β-Lactamase Activities. ChemBioChem 2019, 20, 511. [PubMed: 29718572]

(26). Kim J; et al. Development of carbapenem-based fluorogenic probes for the clinical screening of carbapenemase-producing bacteria. Bioorg. Chem 2020, 94, 103405. [PubMed: 31806156]

(27). Chen C; et al. A protein structure-guided covalent scaffold selectively targets the B1 and B2 subclass metallo-β-lactamases. Chem. Commun 2018, 54, 4802.

(28). Singha M; et al. Rapid Fluorescent-Based Detection of New Delhi Metallo-β-Lactamases by Photo-Cross-Linking Using Conjugates of Azidonaphthalimide and Zinc(II)-Chelating Motifs. ACS Omega 2019, 4, 10891. [PubMed: 31460186]

(29). Brem J; et al. Structural Basis of Metallo-β-Lactamase Inhibition by Captopril Stereoisomers. Antimicrob. Agents Chemother 2016, 60, 142. [PubMed: 26482303]

(30). Yusof Y; Tan DTC; Arjomandi OK; Schenk G; McGeary RP Captopril analogues as metallo-β-lactamase inhibitors. Bioorg. Med. Chem. Lett 2016, 26, 1589. [PubMed: 26883147]

(31). Bai C-G; Xu Y-T; Li N-N; Wang J-H; Yang C; Chen Y; Zhou H-G Cysteine and Its Derivatives as New Delhi Metallo-beta-lactamase-1 Inhibitors. Curr. Enzyme Inhib 2015, 11, 46.

(32). Sainlos M; Imperiali B Synthesis of anhydride precursors of the environment-sensitive fluorophores 4-DMAP and 6-DMN. Nat. Protoc 2007, 2, 3219. [PubMed: 18079722]

(33). Vázquez ME; Blanco JB; Imperiali B Photophysics and biological applications of the environment-sensitive fluorophore 6-N,N-dimethylamino-2,3-naphthalimide. J. Am. Chem. Soc 2005, 127, 1300. [PubMed: 15669870]

(34). Klingler FM; et al. Approved Drugs Containing Thiols as Inhibitors of Metallo-β-lactamases: Strategy To Combat Multidrug-Resistant Bacteria. J. Med. Chem 2015, 58, 3626. [PubMed: 25815530]

(35). Chen AY; et al. Dipicolinic Acid Derivatives as Inhibitors of New Delhi Metallo-β-lactamase-1. J. Med. Chem 2017, 60, 7267. [PubMed: 28809565]

(36). Copeland RA Evaluation of enzyme inhibitors in drug discovery. A guide for medicinal chemists and pharmacologists. Methods Biochem. Anal 2005, 46, 1. [PubMed: 16350889]

(37). Sparta M; Shirvanyants D; Ding F; Dokholyan NV; Alexandrova AN Hybrid dynamics simulation engine for metalloproteins. Biophys. J 2012, 103, 767. [PubMed: 22947938]

(38). Reilley DJ; et al. Toxic and Physiological Metal Uptake and Release by Human Serum Transferrin. Biophys. J 2020, 118, 2979. [PubMed: 32497515]

(39). Nechay MR; Gallup NM; Morgenstern A; Smith QA; Eberhart ME; Alexandrova AN Histone Deacetylase 8: Characterization of Physiological Divalent Metal Catalysis. J. Phys. Chem. B 2016, 120, 5884. [PubMed: 26996235]

(40). Cheng Z A Single Salt Bridge in VIM-20 Increases Protein Stability and Antibiotic Resistance under Low-Zinc Conditions. mBio 2019, 10, e02412–19. [PubMed: 31744917]

(41). Aitha M; et al. Biochemical, Mechanistic, and Spectroscopic Characterization of Metallo-β-lactamase VIM-2. Biochemistry 2014, 53, 7321. [PubMed: 25356958]

(42). Thomas CA; et al. Probing the mechanisms of inhibition for various inhibitors of metallo-β-lactamases VIM-2 and NDM-1. J. Inorg. Biochem 2020, 210, 111123. [PubMed: 32622213]

(43). Chen AY; et al. Investigation of Dipicolinic Acid Isosteres for the Inhibition of Metallo-β-Lactamases. ChemMedChem 2019, 14, 1271. [PubMed: 31124602]

(44). Ju LC; Cheng Z; Fast W; Bonomo RA; Crowder MW The Continuing Challenge of Metallo-β-Lactamase Inhibition: Mechanism Matters. Trends Pharmacol. Sci 2018, 39, 635. [PubMed: 29680579]

(45). Golovine K; Uzzo RG; Makhov P; Crispen PL; Kunkle D; Kolenko VM Depletion of intracellular zinc increases expression of tumorigenic cytokines VEGF, IL-6 and IL-8 in prostate cancer cells via NF-κB dependent pathway. Prostate 2008, 68, 1443. [PubMed: 18615482]

(46). Jackson AC; Zaengle-Barone JM; Puccio EA; Franz KJ A Cephalosporin Prochelator Inhibits New Delhi Metallo-β-lactamase 1 without Removing Zinc. ACS Infect. Dis 2020, 6, 1264. [PubMed: 32298084]

(47). Raushel FM; Holden HM Phosphotriesterase: an enzyme in search of its natural substrate. Adv. Enzymol. Relat. Areas Mol. Biol 2006, 74, 51.

(48). Jeremias HF; et al. Study of the interactions of bovine serum albumin with a molybdenum(II) carbonyl complex by spectroscopic and molecular simulation methods. PLoS One 2018, 13, e0204624. [PubMed: 30261022]

(49). Lee S; et al. Development of Human Serum Albumin Selective Fluorescent Probe Using Thieno[3,2-b]pyridine-5(4H)-one Fluorophore Derivatives. Sensors 2019, 19, 5298.

(50). Yamaguchi Y; et al. A Demetallation Method for IMP-1 Metallo-β-Lactamase with Restored Enzymatic Activity Upon Addition of Metal Ion(s). ChemBioChem 2011, 12, 1979. [PubMed: 21739563]

(51). Rokney A; Shagan M; Kessel M; Smith Y; Rosenshine I; Oppenheim ABE coli transports aggregated proteins to the poles by a specific and energy-dependent process. J. Mol. Biol 2009, 392, 589. [PubMed: 19596340]

(52). Ma G; et al. Structure-guided optimization of D-captopril for discovery of potent NDM-1 inhibitors. Bioorg. Med. Chem 2021, 29, 115902. [PubMed: 33302045]

(53). Chung L; Rajan KS; Merdinger E; Grecz N Coordinative binding of divalent cations with ligands related to bacterial spores. Equilibrium studies. Biophys. J 1971, 11, 469. [PubMed: 5569493]

(54). Radford RJ; Lippard SJ Chelators for investigating zinc metalloneurochemistry. Curr. Opin. Chem. Biol 2013, 17, 129. [PubMed: 23478014]

(55). Vaara M Agents that increase the permeability of the outer membrane. Microbiol. Rev 1992, 56, 395. [PubMed: 1406489]

(56). https://www.ncbi.nlm.nih.gov/pathogens/refgene/-gene_family:(blaNDM) (accessed Dec 17, 2020).

(57). Makena A; et al. Biochemical characterization of New Delhi metallo-β-lactamase variants reveals differences in protein stability. J. Antimicrob. Chemother 2015, 70, 463. [PubMed: 25324420]

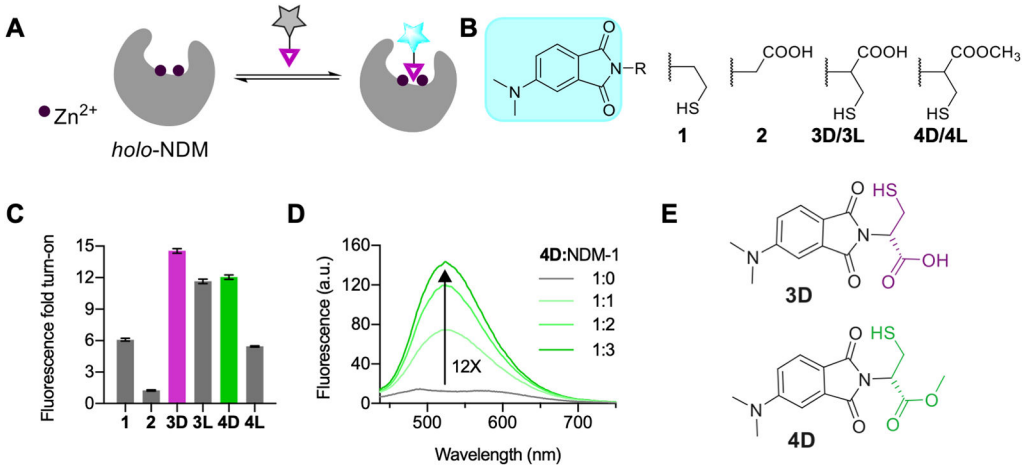

Figure 1.

(A) Design of reversible NDM-1 fluorescent probes. (B) Structures of probes **1–4**. (C) Fluorescence fold turn-on of probes with NDM-1 (1:3 ratio, 10 μM probe; λ_{ex} = 420 nm). (D) Fluorescence spectra showing the fluorescence turn-on for probe **4D** (10 μM) with increasing equivalents of NDM-1. λ_{ex} = 420 nm. (E) Probes showing the best fluorescence response with NDM-1. All studies were conducted in degassed 50 mM HEPES, 10 μM $ZnSO_4$ buffer, pH 7.0, at room temperature using acetonitrile (≤5% v/v) as a cosolvent.

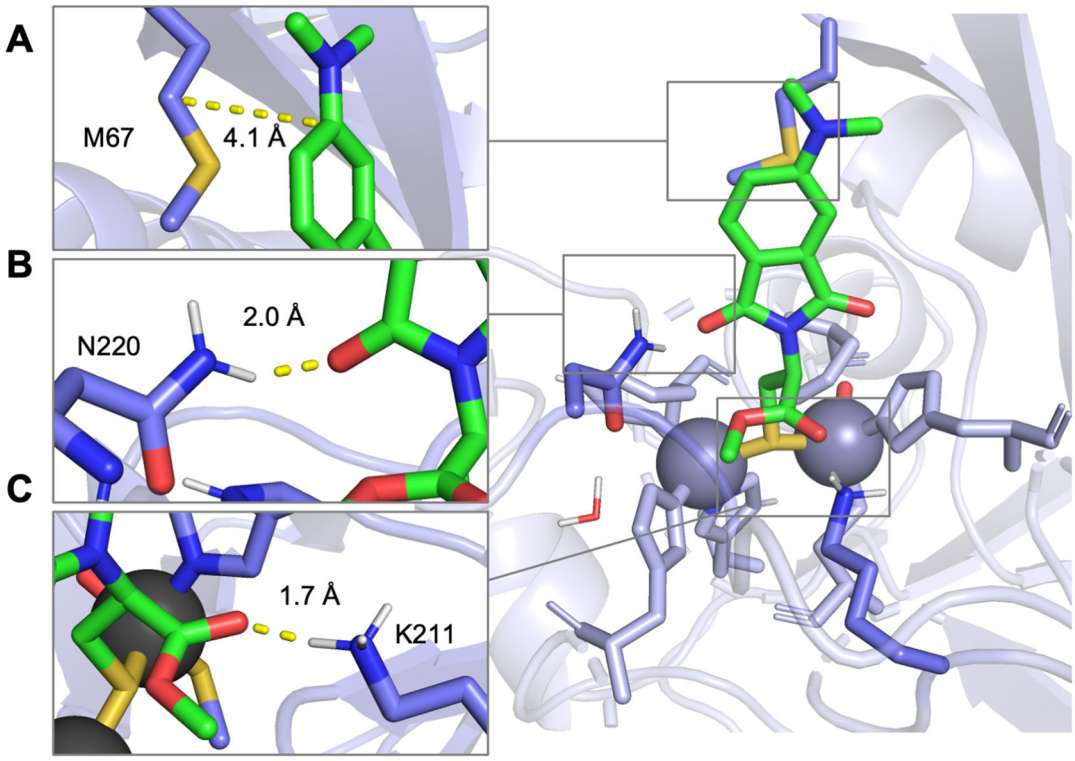

Figure 2.

Proposed binding modes from QM/DMD simulations for probe **4D** with NDM-1 (PDB: 4EXS), with insets showing (A) interactions between the fluorophore end of the probe and hydrophobic M67 in Loop 3. (B) Interaction between N220 and the carbonyl oxygen of the imide ring of the fluorophore. (C) Interaction between K211 and the carbonyl groups in the metal binding group end of the probe.

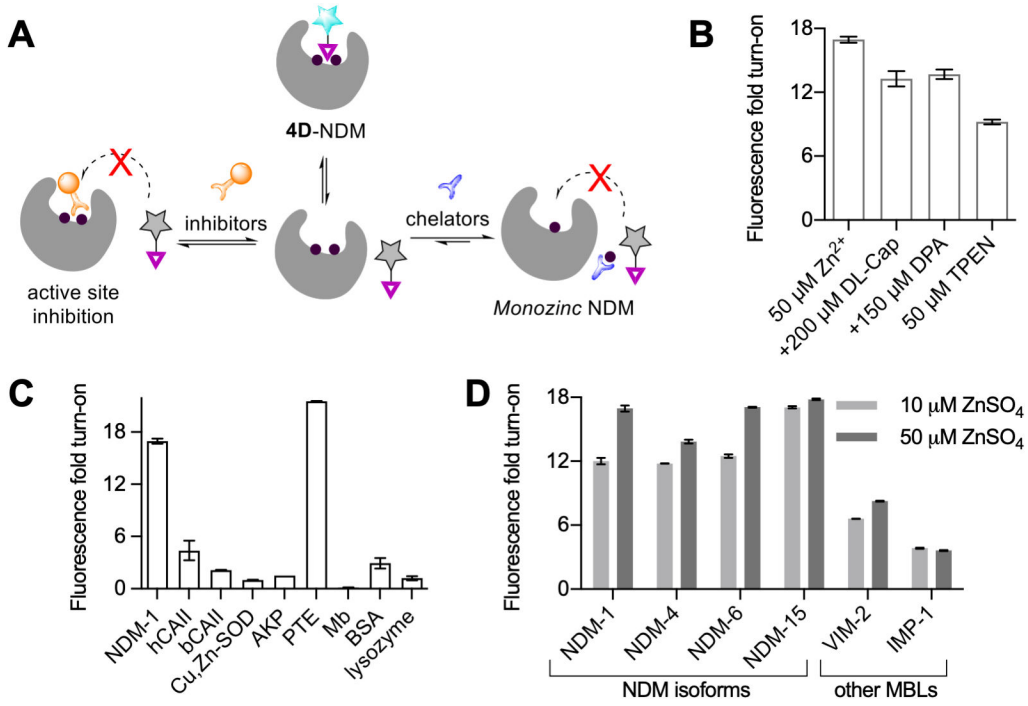

Figure 3.

(A) Schematic showing the effects of chelator and inhibitor treatments on **4D**/NDM-1 mixtures. (B) Change in fluorescence turn-on of **4D**-NDM-1 (1:3, 10 μM probe) upon treatments with $ZnSO_4$ TPEN, DL-captopril (DL-Cap), and dipicolinic acid (DPA). (C) Fluorescence turn-on for **4D** with other proteins (1:3, 10 μM probe), human carbonic anhydrase II (hCAII), bovine carbonic anhydrase II (bCAII), Cu,Zn-superoxide dismutase (Cu,Zn-SOD), alkaline phosphatase (AKP), phosphotriesterase (PTE), myoglobin (Mb), and bovine serum albumin (BSA). (D) Fluorescence turn-on for **4D** with different NDM-1 isoforms and two other metallo-β-lactamases, VIM-2 and IMP-1 (1:3, 10 μM probe), in the presence of 10 μM $ZnSO_4$ (light gray) and 50 μM $ZnSO_4$ (dark gray).

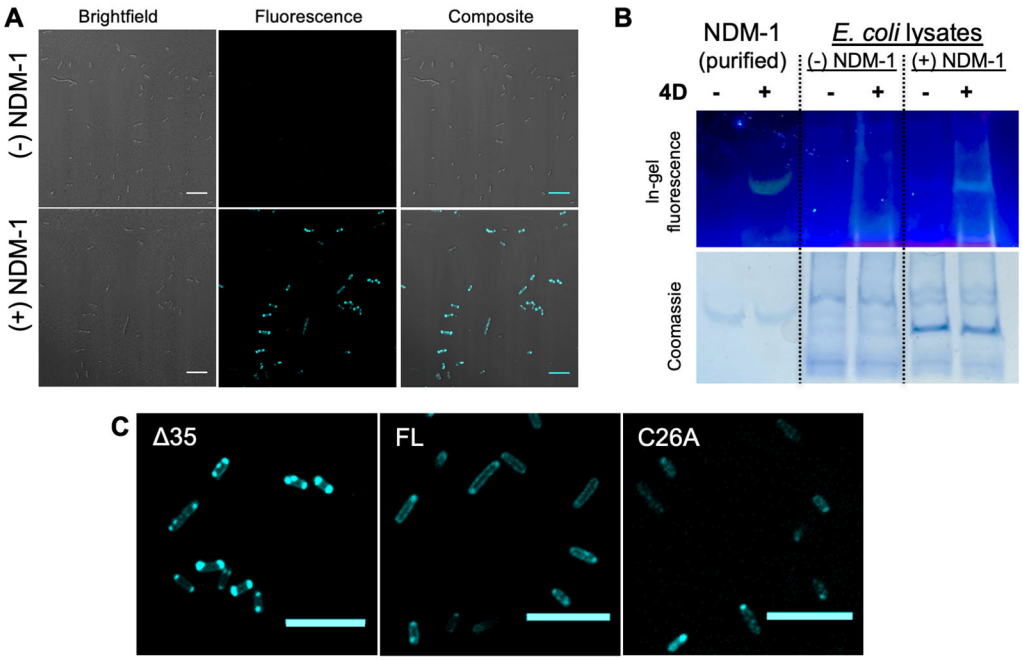

Figure 4.

(A) Confocal fluorescence images of **4D**-treated BL21 cells with the Δ35 construct in the presence and absence of IPTG for NDM-1 expression. (B) In-gel fluorescence (probe **4D**) and Coomassie staining of native SDS-PAGE run at 120 V for 40 min (4–20% gel) with lysates of BL21 (DE3) cells with the Δ35 construct with and without NDM-1 expression. (C) Confocal fluorescence images of BL21 expressing different NDM-1 constructs (Δ35, FL, C26A) stained with **4D** (10 μM). For all imaging experiments, cells were grown in LB broth at 37 °C, supplemented with 0.5 mM IPTG and 50 μM $ZnSO_4$, and protein expression was induced for 2 h. Prior to imaging, the cells were re-suspended in M9 minimal media to obtain a final OD of ~0.3 for imaging. Scale: 10 μm. $\lambda_{ex}/\lambda_{em}$: 405/486–614.

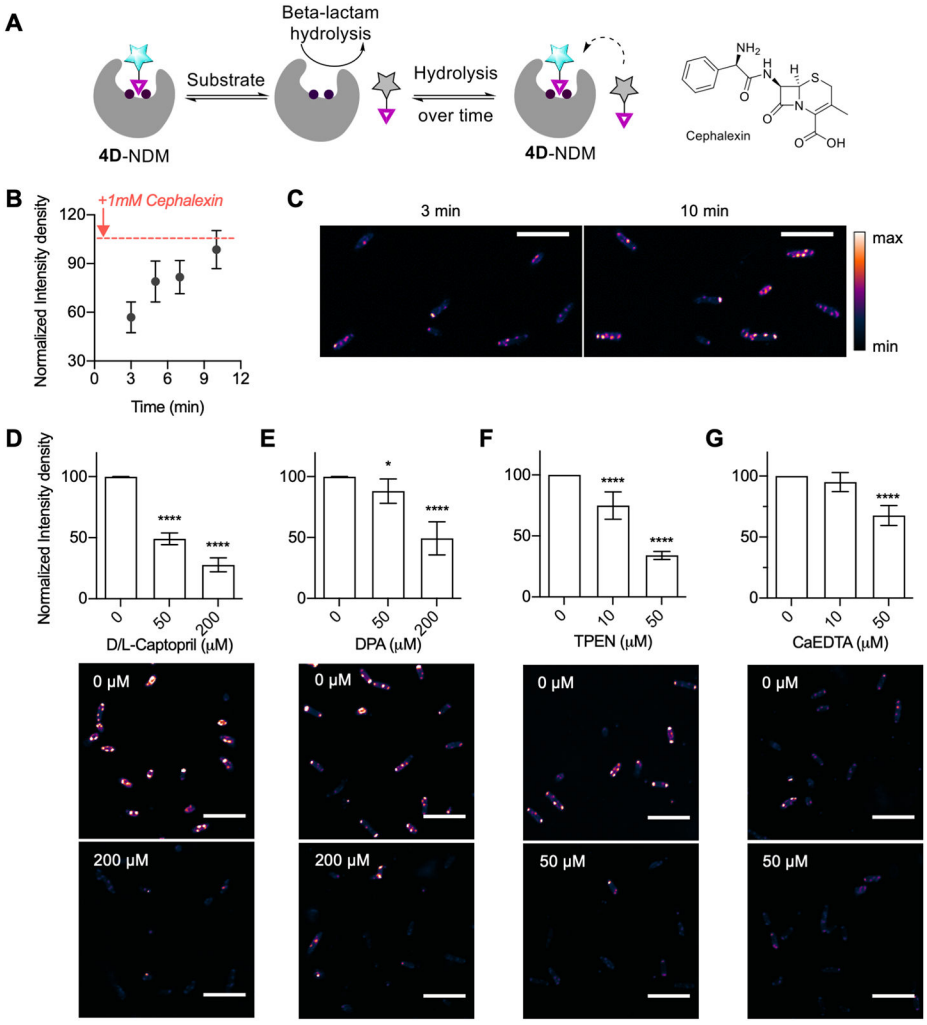

Figure 5.

(A) Schematic showing probe displacement by the substrate and the structure of cephalexin. (B) Time-dependent fluorescence intensity after addition of cephalexin (1 mM) to **4D**-treated *E. coli* BL21 (DE3) expressing Δ35 NDM-1. (C) Example images from 3 min versus 10 min samples used to construct panel B. Effects of DL-captopril (panel D), DPA (panel E), TPEN (panel F), and CaEDTA (panel G) on the fluorescence intensity of BL21 (DE3) cells expressing Δ35 NDM-1 after 20 min incubation (5 min with 8 μM **4D**, followed by 15 min of treatment with indicated additives). All data were recorded in triplicate and analyzed using two-way ANOVA (*$p < 0.05$, **$p < 0.01$, ***$p < 0.001$, ****$p < 0.0001$). Scale bar: 10 μm. $\lambda_{ex}/\lambda_{em}$: 405/486–614. All statistical analyses are indicating statistics with respect to the 0 μM treatment.

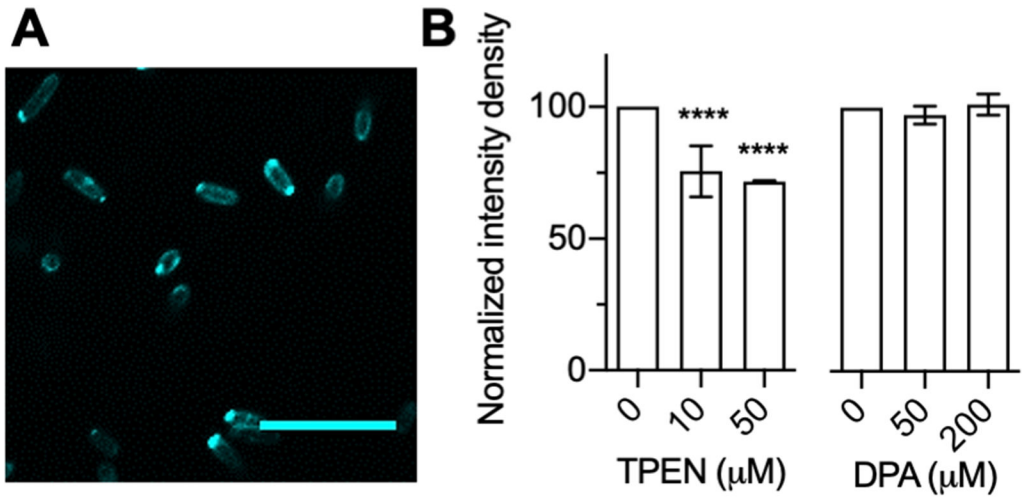

Figure 6.

(A) Fluorescence image showing expression and localization of NDM-15 cellular Δ35 construct with probe **4D**. (B) Effect of addition of TPEN and DPA to NDM-15 Δ35 BL21 cells. All data were recorded in triplicate (2–3 different trials), and two-way ANOVA was performed to determine significance (****$p < 0.0001$). Scale bar: 10 μm. $\lambda_{em}/\lambda_{em}$: 405/486–614. All statistical analyses are indicating statistics with respect to the 0 μM treatment.

Table 1.

Minimum Values for Binding Penalties, Metal Angle Variances, and Distances for Probes 3D and 4D[a]

	minimum values		distances (Å)			
probe	binding penalties (kcal/mol)	metal angle variance (deg)	(thiol) S–Zn1	(thiol) S–Zn2	(carboxyl) O– NH (K211)	(carbonyl) O– NH (N220)
3D	10.5	7.96	2.3	2.4	1.8	2.5
4D	4.2	7.52	2.3	2.4	1.7	2.0

[a]We employed lowest binding energy mode 2 of the QM/DMD model for these data (Figures S17-S20).